Title

Gastric Metabolomics Detects Helicobacter pylori Correlated Loss of Numerous Metabolites in Both the Corpus and Antrum.

Journal

Infection and Immunity, 89(2)

ISSN

0019-9567

Authors

Keilberg, Daniela
Steele, Nina
Fan, Sili
et al.

Publication Date

2021-01-19

DOI

10.1128/iai.00690-20

Peer reviewed

AMERICAN SOCIETY FOR MICROBIOLOGY | Infection and Immunity®

BACTERIAL INFECTIONS

Gastric Metabolomics Detects *Helicobacter pylori* Correlated Loss of Numerous Metabolites in Both the Corpus and Antrum

Daniela Keilberg,[a] Nina Steele,[b*] Sili Fan,[c] Christina Yang,[a] Yana Zavros,[b*] Karen M. Ottemann[a]

[a]Department of Microbiology and Environmental Toxicology, University of California, Santa Cruz, California, USA
[b]Department of Pathology and Lab Medicine, University of Cincinnati College of Medicine, Cincinnati, Ohio, USA
[c]West Coast Metabolomics Center, University of California Davis, Davis, California, USA

ABSTRACT *Helicobacter pylori* is a chronic bacterial pathogen that thrives in several regions of the stomach, causing inflammation that can vary by site and result in distinct disease outcomes. Whether the regions differ in terms of host-derived metabolites is not known. We thus characterized the regional variation of the metabolomes of mouse gastric corpus and antrum organoids and tissue. The uninfected secreted organoid metabolites differed between the corpus and antrum in only seven metabolites as follows: lactic acid, malic acid, phosphoethanolamine, alanine, uridine, glycerol, and isoleucine. Several of the secreted chemicals were depleted upon *H. pylori* infection in both regions, including urea, cholesterol, glutamine, fumaric acid, lactic acid, citric acid, malic acid, and multiple nonessential amino acids. These results suggest a model in which *H. pylori* preferentially uses carboxylic acids and amino acids in complex environments, and these are found in both the corpus and antrum. When organoid metabolites were compared to mouse tissue, there was little overlap. The tissue corpus and antrum metabolomes were distinct, including antrum-elevated 5-methoxytryptamine, lactic acid, and caprylic acid, and corpus-elevated phospholipid products. The corpus and antrum remained distinct over an 8-month infection time course. The antrum displayed no significant changes between the time points in contrast to the corpus, which exhibited metabolite changes that were consistent with stress, tissue damage, and depletion of key nutrients, such as glutamine and fructose-6-phosphate. Overall, our results suggest that the corpus and antrum have largely but not completely overlapping metabolomes that change moderately upon *H. pylori* infection.

KEYWORDS carbon metabolism, gastric, organoid

The mammalian body is colonized by a rich diversity of bacteria that can utilize a range of nutrients. To establish long-term colonization, bacteria must sense and adapt to nutrient conditions that likely vary temporally and spatially. One bacterium that can establish a chronic infection is *Helicobacter pylori*, which colonizes two main stomach regions, the corpus, also called the fundus in mice, and the antrum. Little is known about the nutrients *H. pylori* utilizes in these two regions and how they vary over space and time.

H. pylori colonizes the stomachs of many people, 50% worldwide and 35% in the United States (1). The infection is acquired in childhood and becomes chronic and persistent unless treated with antibiotics. Approximately 85% of infected people are asymptomatic, developing only a low-level inflammation. However, around 15% of infected people will develop serious *H. pylori* triggered disease during their life, either a gastric or duodenal ulcer or gastric cancer (2, 3).

The corpus and antrum are the two main stomach regions in both mice and humans and are distinct from each other in several ways. In each of these regions, the

Citation Keilberg D, Steele N, Fan S, Yang C, Zavros Y, Ottemann KM. 2021. Gastric metabolomics detects *Helicobacter pylori* correlated loss of numerous metabolites in both the corpus and antrum. Infect Immun 89:e00690-20. https://doi.org/10.1128/IAI.00690-20.

Editor Victor J. Torres, New York University School of Medicine

Address correspondence to Karen M. Ottemann, ottemann@ucsc.edu.

* Present address: Nina Steele, Department of Cell and Developmental Biology, University of Michigan, Ann Arbor, Michigan, USA; Yana Zavros, Department of Cellular and Molecular Medicine, University of Arizona, Tucson, Arizona, USA.

Received 29 October 2020
Accepted 31 October 2020
Accepted manuscript posted online 9 November 2020
Published 19 January 2021

epithelium is highly invaginated into gastric glands that each contain stem cells (4, 5). These stem cells give rise to a distinct set of epithelial cells in each area. Both areas contain cells that secrete mucus apically, but the corpus is specialized for digestive functions while the antrum is specialized for endocrine ones (6). The corpus digestive functions are created via acid-secreting parietal cells along with pepsinogen- and lipase-secreting chief/zymogenic cells, all secreted apically. The antrum endocrine function is created by gastrin-producing G cells, which are secreted basolaterally. Overall, these different cell types create a distinct milieu in each region, which might require distinct *H. pylori* abilities for colonization. There is some support for this idea, as *H. pylori* mutants lacking chemotaxis have a greater colonization defect in the antrum than in the corpus (7–9), while mutants lacking the cytotoxin-associated pathogenicity island (*cag*PAI) genes *cagA* or *cagY* have a greater colonization defect in the corpus than in the antrum (10). However, the nature of the differences that *H. pylori* encounters in these two regions is not known.

Several studies have compared *H. pylori* mouse colonization dynamics between the corpus and antrum (8, 9). *H. pylori* infections begin corpus dominant with 5- to 10-fold larger amounts than the antrum. Over the first 2 months, however, *H. pylori* multiplies to a great extent in the antrum, such that the infection becomes antral dominant from 1 week postinfection to ~2 months postinfection (8, 9). After 2 months of infection, the *H. pylori* numbers decline more in the antrum, and the infection becomes corpus dominant again. These experiments suggest that the antrum switches between a challenging and favorable environment for *H. pylori* growth. In agreement with this idea, bacterial chemotaxis, the ability to sense environmental conditions and move toward beneficial ones and away from harmful ones, is particularly critical in the antrum (7, 9). Overall, these colonization patterns suggest that host metabolites might differ between the corpus and the antrum and possibly change over the course of the infection.

Knowledge about the corpus and antrum conditions is important because *H. pylori*-triggered diseases differ in these two areas. Inflammation localized to the antrum leads mainly to ulcers and few cancers, inflammation in the corpus correlates with intestinal-type gastric cancer, and inflammation throughout the stomach increases the risk of diffuse-type gastric cancer (3, 11, 12). It is not known whether there are metabolite differences between these regions. Metabolomics studies of gastric tissue have been limited. The total mouse gastric metabolome was analyzed over an *H. pylori* infection time course, but the separate corpus and antrum metabolites were not characterized (13). These authors did find evidence of upregulation of glycolysis, TCA, and choline pathway intermediates, but the findings were not consistent across time points. Other studies have compared the metabolomes of human gastric cancerous and normal tissue (reviewed in reference 14), in part with the idea that these metabolites might be biomarkers of disease (15). Those studies were noted to have limitations but *in toto* suggested that cancerous tissue has elevated amounts of lactic acid, citric acid, fumaric acid, glutamine, glutamate, and valine as well as several free fatty acids. To help fill gaps in our knowledge, we thus embarked on a study of the metabolomes of mouse gastric corpus and antrum organoids and tissue to describe them and evaluate how *H. pylori* infection affected them. We report here that a handful of metabolites differ between these compartments. Several are depleted upon *H. pylori* infection and, thus, may represent *H. pylori* nutrient sources. We additionally find that the antrum is surprisingly stable preinfection and postinfection while the corpus undergoes substantial alterations. Overall, our results are consistent with *H. pylori* preferential catabolism of carboxylic acids and amino acids in both the corpus and the antrum.

RESULTS

Comparison of the secreted metabolites of antrum and corpus organoids. We investigated the differences in corpus/fundus and antrum first using a mouse organoid system because this approach would allow us to isolate secreted metabolites that would be accessible to *H. pylori*. For this experiment, mouse gastric glands were

isolated from the corpus or antrum and then cultured as spherical organoids. This culture method results in representation of all standard stomach epithelial cells, including surface pit, mucous neck, chief, endocrine, and parietal cells (16). After development of spheroids, the organoids were transferred to collagen-coated dishes to allow them to flatten out as two-dimensional (2D) organoids. The 2D organoid culture medium is very rich and contains tissue culture medium (Dulbecco modified Eagle medium [DMEM]), fetal bovine serum (FBS), and multiple growth factor supplements. For metabolomics analysis, the culture supernatant was collected, filtered to remove cells, and analyzed using gas chromatography-time of flight (GC-TOF) mass spectroscopy for various metabolites, including carbohydrates, sugar phosphates, amino acids, hydroxyl acids, free fatty acids, purines, and pyrimidines. Control samples included medium alone. Difference comparisons between two groups were made using Student's *t* test and between multiple groups using a one-way analysis of variance (ANOVA) with a false-discovery rate (FDR) *P* value adjustment using the Benjamini-Hochberg procedure (17). We refer to these differences as significant or highly significant, respectively.

Using this approach, a total of 352 compounds were found to be secreted by the organoids, of which 132 (38%) were identified chemicals while the other 220 (62%) were unknown chemical structures (see Table S1 in the supplemental material). Principal-component analysis (PCA) suggested that the organoid supernatant differed only minimally from the medium (Fig. 1A), which was consistent with the richness of the organoid medium. The corpus organoid supernatant had no highly significant differences from medium, while the antrum organoid supernatant had 13 highly significant differences (see Table S2 in the supplemental material). Nine of these chemicals were decreased in the organoid supernatant compared to the medium, including the amino acids aspartic acid, leucine, serine, isoleucine, phenylalanine, and valine and the chemicals glycerol, ethanolamine, and nicotinamide (Table S2). Three metabolites were significantly elevated 1.7- to 3.9-fold by the antral organoid system, suggesting that they may be excreted or released by the cells. These were the carboxylic acids lactic acid and malic acid and the phospholipid component phosphoethanolamine (Table S2). This analysis thus suggests that medium collected after exposure to corpus organoids did not change much in composition, while exposure to antral organoids lead to a significant increase of lactic acid, malic acid, and phosphoethanolamine.

We next compared the antrum and corpus organoids to each other (Fig. 2). Twenty-six named compounds differed between the two, with seven of these being highly significant (Fig. 2; see also Table S3 in the supplemental material). Antral organoids were significantly enriched over the corpus organoids for lactic acid, malic acid, fumaric acid, alanine, and phosphoethanolamine. Corpus organoids were enriched for the pyrimidine nucleoside uridine, glycerol, and the amino acid isoleucine. For the most part, these differences were not more than 2-fold, except for higher antrum enrichment for lactic acid and phosphoethanolamine (Fig. 2). Given these modest differences, principal-component analysis did not substantially separate the uninfected corpus and antrum organoid supernatants (Fig. 1A). ChemRICH chemical similarity analysis (18) was used to identify the significantly impacted metabolic clusters in our data. This analysis uses the larger set of non-FDR-corrected significant compounds and fold changes. As shown in Fig. 1B, the significant corpus-antrum organoid differences were clustered into three metabolite groups as follows: general amino acids, branched-chain amino acids, and dicarboxylic acids (Fig. 1B). These analyses show that corpus and antrum organoid supernatants display some differences from each other, dominated by the antral presence of carboxylic acids and phosphoethanolamine.

Antrum and corpus organoid supernatants show a metabolite change in response to *H. pylori* infection. We next examined how the antrum and corpus organoid supernatants changed after *H. pylori* infection. Both types of organoids support *H. pylori* colonization (19, 20). After preparation, the 2D organoids were infected by adding the mouse-adapted wild-type *H. pylori* strain SS1 to the medium. Infections proceeded for

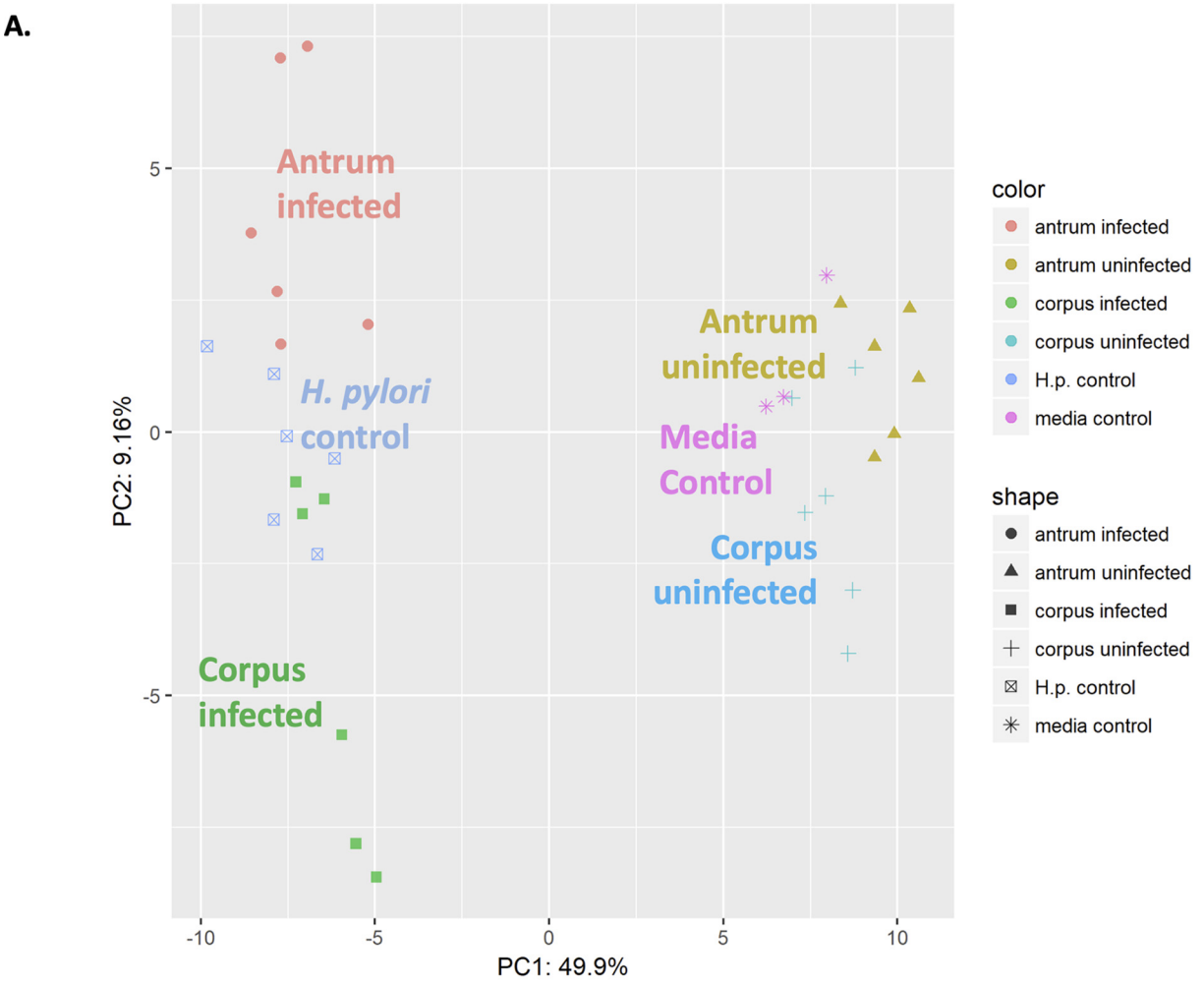

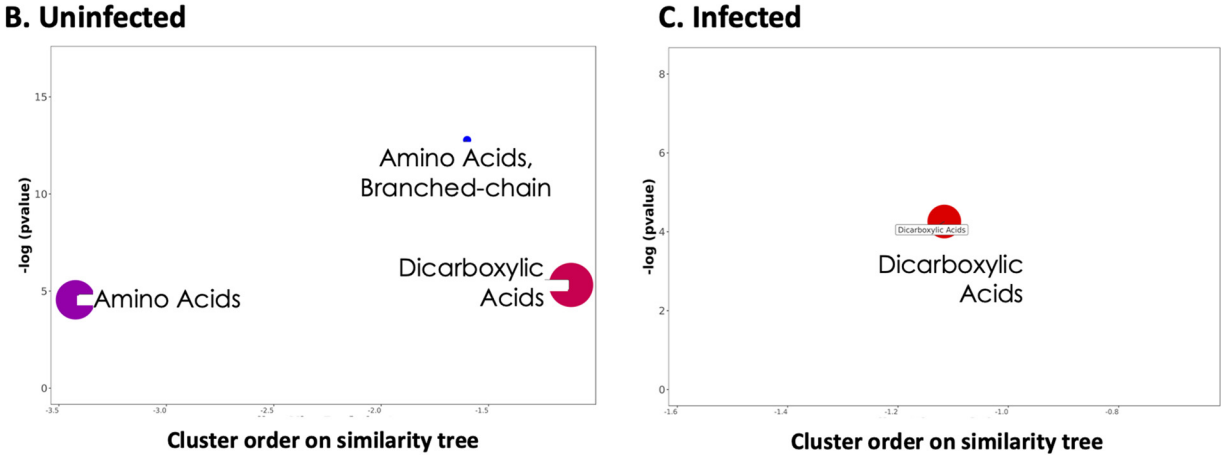

FIG 1 Comparison of metabolites from 2D organoid culture supernatants of mouse gastric antrum and corpus with and without infection by *H. pylori* SS1. Control samples include organoid medium alone and *H. pylori* alone. (A) Principle-component analysis (PCA). (B and C) ChemRICH enrichment analysis comparing either the uninfected or infected corpus and antrum for pairwise comparison, as detailed in Table S4 in the supplemental material. The *y* axis shows the most significantly altered clusters at the top, with enrichment *P* values given by the Kolmogorov-Smirnov test. Only enrichment clusters are shown that are significantly different at a *P* value of <0.05. The *x* axis shows clusters that are generated by chemical similarity and ontology mapping. Each node reflects a significantly altered cluster of metabolites. Node sizes represent the total number of metabolites in each cluster set. The node color scale shows the proportion of increased (red) or decreased (blue) compounds or both increased and decreased metabolites (purple). For each sample, $n = 6$ except media alone where $n = 3$.

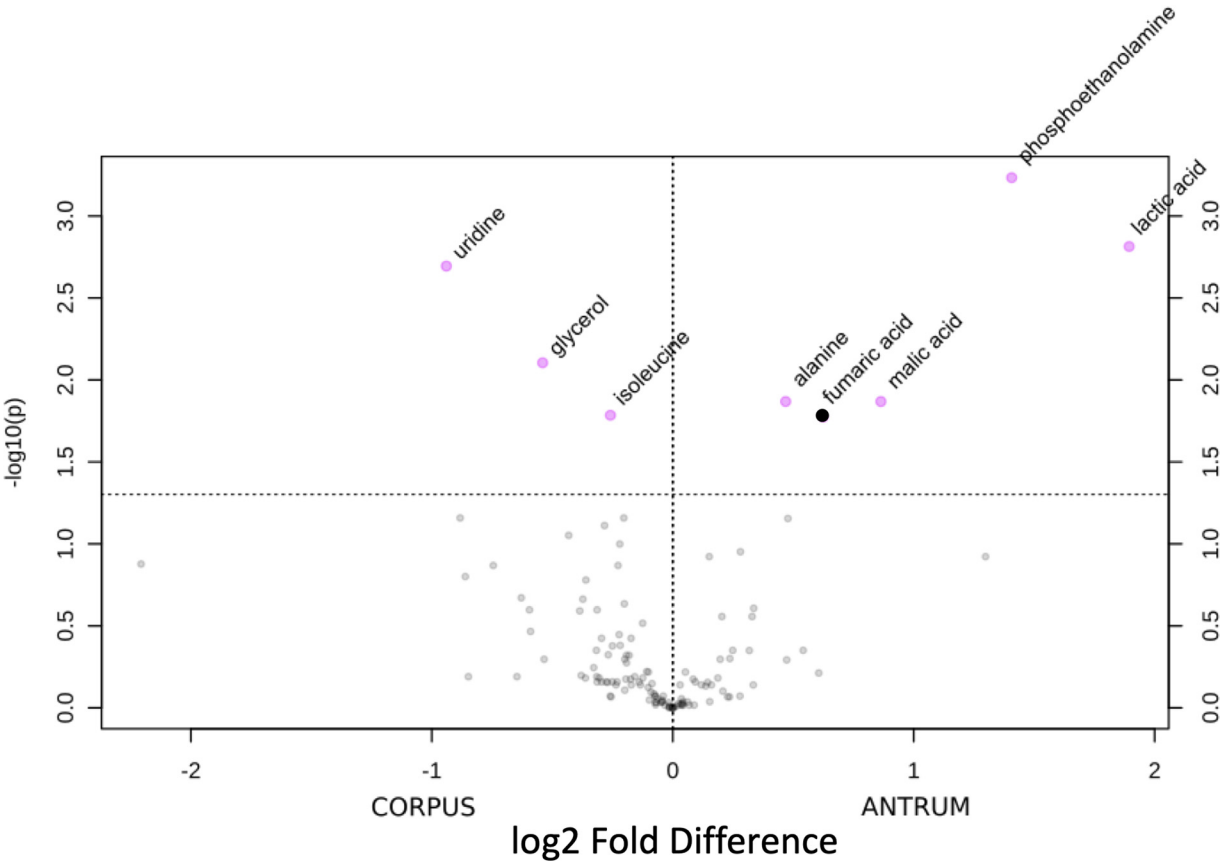

FIG 2 Volcano plot comparing organoid supernatant from uninfected corpus and uninfected antrum. Named compounds that differed significantly are labeled; those with significant FDR-corrected *P* values have a pink dot, and one just below significance has a black dot (see Table S3 in the supplemental material). Uninfected gastric organoid supernatant was collected and analyzed for total metabolites. $n = 6$ for each group.

24 h, and then the supernatant was collected, filtered to remove all cells, and analyzed as above. Controls were the same amounts of *H. pylori* incubated in organoid medium lacking organoids as well as organoid medium by itself. *H. pylori* infection resulted in a highly significant change of 46 antrum supernatant chemicals (Table 1) and 88 total significant chemicals (see Table S5 in the supplemental material). Similarly, infection of corpus organoids resulted in a highly significant change of 51 chemicals in the supernatant (Table 2) and 101 total significant ones (see Table S6 in the supplemental material). Changes in both types of organoid supernatants mapped to multiple categories of metabolites but most substantially to amino acids and dicarboxylic acids and additionally sugar alcohols in the corpus (see Fig. S1 in the supplemental material). These changes resulted in a substantial shift in the principal components between uninfected and infected samples (Fig. 1A).

Several of the changed metabolites were depleted with *H. pylori* infection (Fig. 3), and these metabolites generally agree with what is known about *H. pylori* metabolism. For example, urea was highly depleted in both corpus and antrum systems (Fig. 3; Table 1 and 2). This decrease agrees with *H. pylori*'s robust urease and its known ability to find urea via chemotaxis (21, 22). Similarly, glutamine was highly depleted, consistent with *H. pylori*'s gamma glutamyl transferase (GGT), which breaks glutamine into glutamate and ammonia (23, 24). Lactic acid was highly depleted in each system too, consistent with *H. pylori*'s ability to use lactic acid as a carbon or energy source (25, 26). Additional amino acids or amino acid derivatives were substantially depleted as well, including serine, *N*-acetylglutamate, aspartic acid, oxoproline/pyroglutamic acid, and tyrosine. Only one of these is an essential amino acid, serine, and only for some strains (27). The other amino acids may be used as *H. pylori* carbon and nitrogen sources as has been

TABLE 1 Compounds that differed significantly between infected and uninfected antral organoid supernatant[a]

Metabolite	Ratio infected to uninfected	FDR-corrected *P* value
Urea	0.04	0.00000
Glutamine	0.10	0.00010
Malic acid	0.23	0.00001
N-acetylglutamate	0.23	0.00036
Serine	0.34	0.00007
Fumaric acid	0.36	0.00010
Lactic acid	0.40	0.05266
Citric acid	0.44	0.00000
Cholesterol	0.51	0.00612
Aspartic acid	0.65	0.03809
Oxoproline	0.74	0.03809
Tyrosine	0.78	0.01238
Isoleucine	1.45	0.00314
Inosine	1.50	0.01138
Threonine	1.53	0.00040
Myristic acid	1.55	0.03049
Ethanolamine	1.59	0.00218
Asparagine	1.64	0.00011
Tryptophan	1.67	0.00727
Valine	1.67	0.00091
Ribose	1.88	0.00001
5-Methoxytryptamine	1.89	0.00230
Glyceric acid	1.89	0.01138
Succinic acid	2.03	0.00001
Pseudouridine	2.05	0.03397
Phenylalanine	2.07	0.00009
Alanine	2.09	0.00002
Leucine	2.11	0.00001
Glycine	2.26	0.00064
Glycerol-alpha-phosphate	2.54	0.02841
Citramalic acid	2.76	0.00010
Uracil	3.00	0.00262
Pyruvic acid	3.06	0.00010
Thymidine	3.13	0.00006
Glycerol	3.57	0.00002
Uric acid	4.41	0.00006
Homoserine	5.02	0.00001
Cysteine	5.34	0.00603
Uridine	5.81	0.00000
Cystine	5.82	0.00006
Xanthine	7.58	0.00225
Lysine	9.08	0.00120
Glutamate	9.68	0.00000
Histidine	12.79	0.00007
Methionine	14.41	0.01977
Taurine	43.87	0.00719

[a]Antral organoids were cultured as 2D organoids and infected with wild-type *H. pylori* SS1 for 24 h. After infection, the culture supernatant was collected and filtered to remove bacteria and mammalian cells. *P* values are corrected for multiple comparisons using the Benjamini-Hochberg procedure. $n = 6$ samples/organoid group and 3 for the *H. pylori* and medium controls.

shown for aspartic acid (28). Also used up were several additional carboxylic acids, including malic acid, fumaric acid, and citric acid (Fig. 3).

Overall, the metabolite usage was similar but nonidentical between the corpus and antrum organoids (Fig. 4). For example, cholesterol, a requirement for *H. pylori* growth (29, 30), was substantially depleted in infected antrum organoids but not corpus organoids (Fig. 4), although it was present in both. Additionally, there were several compounds that were lowered more in the corpus, including the carboxamide lactic acid derivative lactamide, the saturated medium-chain fatty acid capric acid (also called decanoic acid), benzoic acid, the sugar alcohol threitol, and the purine guanosine (Fig. 4). Again, these compounds were present in both organoids but were not highly lessened in the antrum. Overall, these results suggest that *H. pylori* infection leads to

TABLE 2 Compounds that differed significantly between infected and uninfected corpus organoid supernatant[a]

Metabolite	Ratio infected to uninfected	FDR-corrected *P* value
Lactic acid	0.01	0.00000
Urea	0.02	0.00000
Glutamine	0.06	0.00000
Aspartic acid	0.17	0.00001
Lactamide	0.27	0.00001
N-acetylglutamate	0.31	0.00035
Malic acid	0.32	0.00000
Serine	0.36	0.00006
Fumaric acid	0.39	0.00193
Capric acid	0.52	0.01265
Citric acid	0.53	0.00007
Tyrosine	0.60	0.00042
Benzoic acid	0.62	0.01764
Oxoproline	0.65	0.00027
Threitol	0.81	0.02178
Guanosine	0.81	0.02083
Isoleucine	1.17	0.02577
Threonine	1.21	0.02849
Oxalic acid	1.22	0.04623
Stearic acid	1.23	0.04208
Inosine	1.33	0.00723
1-Monostearin	1.34	0.04585
Valine	1.36	0.00072
Phenylalanine	1.45	0.03142
Myristic acid	1.48	0.01723
Phosphoethanolamine	1.51	0.00293
Hypoxanthine	1.52	0.03807
Glycine	1.53	0.00049
Glycerol-alpha-phosphate	1.56	0.00738
Glyceric acid	1.61	0.00098
Pseudouridine	1.61	0.00788
Leucine	1.65	0.00065
Sucrose	1.91	0.01583
Glycerol	1.99	0.03715
5-Methoxytryptamine	2.00	0.00009
Ribose	2.01	0.00024
2-Hydroxyglutaric acid	2.06	0.00392
Alanine	2.17	0.00002
Succinic acid	2.19	0.00002
Thymidine	2.48	0.00006
Uric acid	2.52	0.04075
Uracil	2.56	0.01117
Homoserine	3.39	0.00039
Thymine	3.81	0.00000
Uridine	3.94	0.00002
Cystine	7.75	0.00000
Xanthine	7.83	0.00008
Glutamate	11.52	0.00000
Taurine	11.87	0.00077
Lysine	12.66	0.00000
Histidine	16.62	0.00000

[a]Corpus organoids were cultured as 2D organoids and infected with wild-type *H. pylori* SS1 for 24 h. After infection, the culture supernatant was collected and filtered to remove cells. *P* values are corrected for the multiple comparison problem using the Benjamini-Hochberg procedure. $n = 6$ samples/organoid group and 3 for the *H. pylori* and medium controls. Of the increased compounds, none differed between the infected corpus organoids and *H. pylori* alone.

depletion of multiple metabolites in both corpus and antrum organoids, many of which are known nutrients and growth substrates, with some region-specific utilization.

Several compounds were increased in infected organoids compared to uninfected ones (Table 1 and 2). Additional insight into these compounds was gained from comparison to *H. pylori* culture supernatant from bacteria grown without organoids. By comparing this sample to the organoid supernatant samples, it seemed that the vast

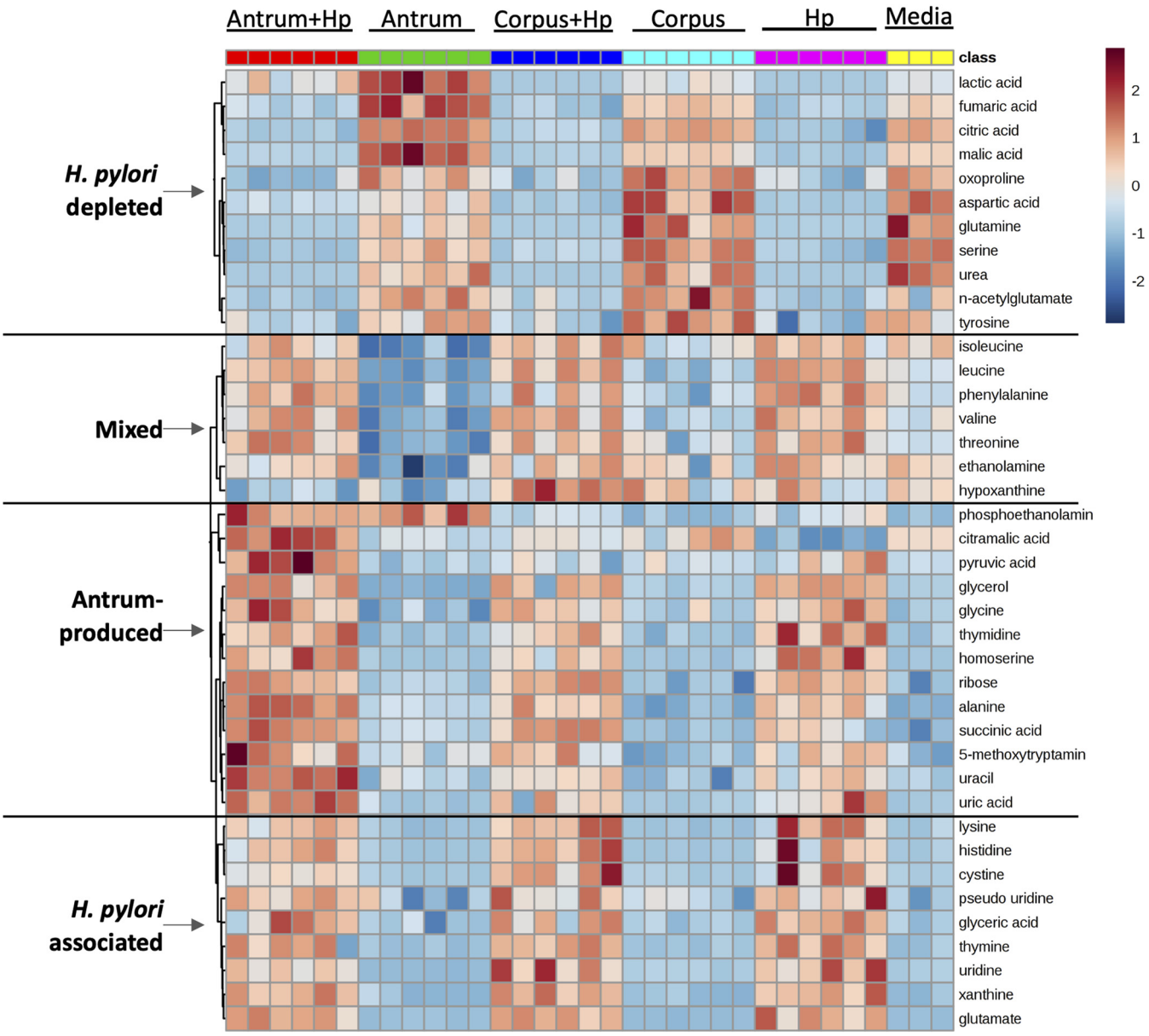

FIG 3 Heat map showing metabolite alterations in organoid supernatant following *H. pylori* infection. The sample sets are listed across the top and include antral organoids supernatant after 24 h exposure to *H. pylori* (Antrum+Hp), antral organoids supernatant alone (Antrum), corpus organoids supernatant after 24 h exposure to *H. pylori* (Corpus+Hp), corpus organoids supernatant alone (Corpus), *H. pylori* spent filtered media (Hp), organoid media (Media). The heat map was generated using MetaboAnalyst 3.0 (53) to show the top 40 most significantly changed compounds identified by ANOVA across groups. Left side labels indicate a description of the major nodes as follows: (i) *H. pylori* depleted, compounds present in the antrum of corpus organoid supernatant whose abundance was less plus *H. pylori*; (ii) Mixed, compounds that did not show a clear pattern; (iii) Antrum-produced, compounds that became more abundant in the antrum organoid supernatant plus *H. pylori*; (iv) *H. pylori*-associated, compounds that were present in the *H. pylori* spent medium.

majority of the increased organoid supernatant compounds were also found in the sample of *H. pylori* alone. This outcome suggests that the increased compounds may have come from *H. pylori*, although they were significantly elevated in the organoid coculture samples (Fig. 3).

After infection, corpus and antrum organoids were more distinct from each other than before infection as seen by a shift and separation of the principle components (Fig. 1A), although the number of highly significantly different metabolites was about the same before and after infection (see Table S3 and S7 in the supplemental material). After infection, there were seven significantly differing compounds that were all found in higher levels in the antrum than in the corpus. The most striking change was in lactic

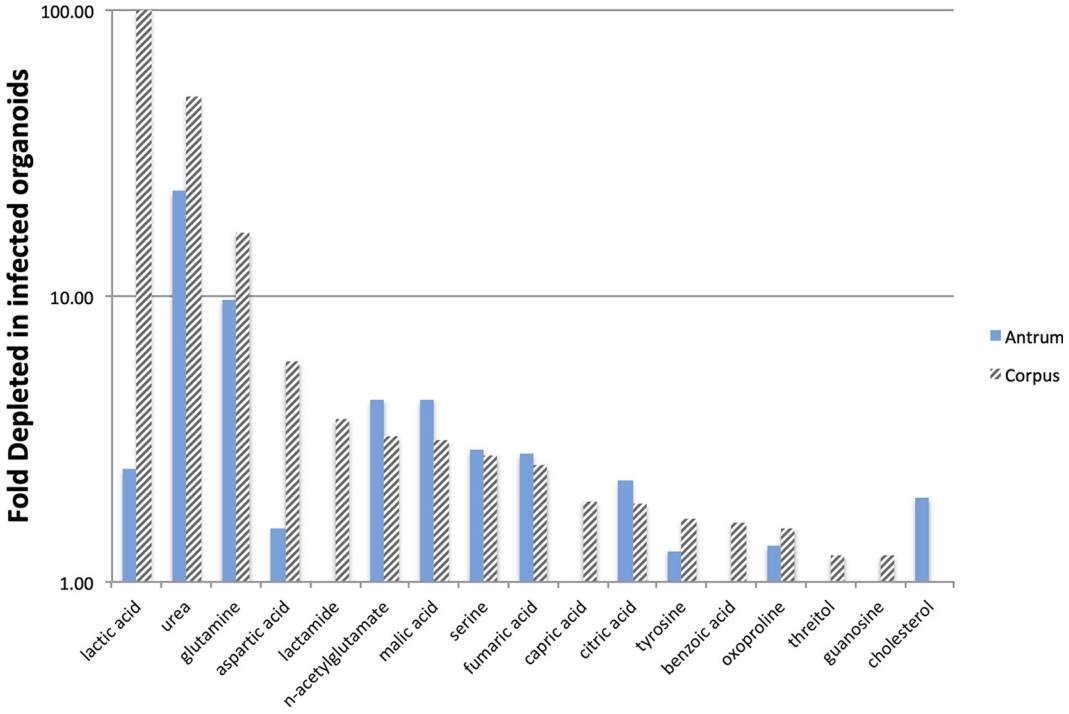

FIG 4 Comparison of compounds depleted from corpus and antrum organoid supernatants with *H. pylori* infection.

acid, which was 150-fold more abundant in the antrum compared to only 3.7-fold more abundant before infection. Phosphoethanolamine also remained enriched in the antrum, remaining about 2-fold greater than in the corpus. The antrum was newly enriched for lactamide, uracil, and citramalic acid (Table S7). Employing ChemRICH enrichment analysis suggested that substantial differences in amino acids were lost and that differences were dominated by those in dicarboxylic acids (Fig. 1C). Overall, these analyses suggest that *H. pylori* infection decreases a discrete set of organoid-secreted metabolites, dominated by urea, glutamine, lactic acid, fumaric acid, citric acid, and specific amino acids. For the most part, these are depleted similarly but nonidentically between the types of organoids with more depletion in the corpus. This differential resulted in the postinfection metabolomes differing from the preinfection metabolomes.

The uninfected mouse tissue differs between antrum and corpus. We next assessed how the metabolome of uninfected mouse gastric tissue compared with that of the gastric organoids analyzed above. First, mouse gastric tissue had substantially fewer total compounds than organoids, with 194 total compounds in the gastric tissue compared with 352 in the organoids (see Table S8 in the supplemental material). A somewhat higher percentage of the tissue metabolites were known—52% in the tissue compared to 38% in the organoids (Table S8). Between the two regions, there were 16 identified compounds that differed with high significance (Fig. 5), a number that was about 2-fold greater than the number of metabolites that were different between the uninfected antrum and corpus organoids (Fig. 2). Generally, most of these differing compounds were enriched in the antrum (Fig. 5). Specifically, the antrum was enriched for several compounds used by *H. pylori* in the organoids, including lactic acid as well as other compounds that did not reach significance (glutamine, capric acid, and benzoic acid) (see Table S9 in the supplemental material).

When comparing the metabolites of the gastric tissue to the metabolites of the organoids, there was not substantial overlap (Tables S1 and S9). This lack of similarity is perhaps not surprising, as the mouse tissue sample was a whole sample, not restricted to secreted molecules. Additionally, the cultured organoid cells are fed

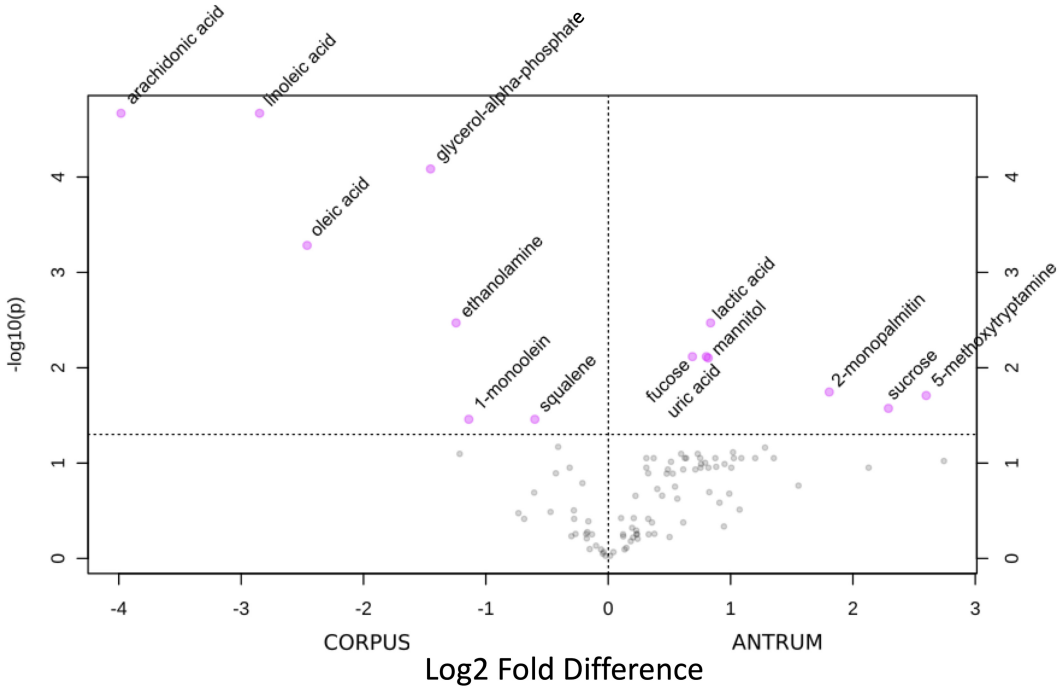

FIG 5 Volcano plot comparing mouse tissue samples from uninfected corpus and uninfected antrum. Compounds with significant FDR-corrected *P* values are labeled. Not shown are octadecanol and dodecanol, which are 2.43 and 2.03 enriched in the antrum. $n = 6$ for each group.

predominantly glucose and glutamine, which may be different than their *in vivo* metabolism. Therefore, it may be that *H. pylori* is exposed to different metabolites in the organoid and tissue settings.

The corpus and antrum mouse tissue remain distinct postinfection. We then infected mice and evaluated how the metabolomes changed over time. We chose time points postinfection that represent different stages of *H. pylori* growth as follows: early rapid (3 days), early steady state (28 days), and late/chronic (8 months). Successful infection was confirmed by plating (Fig. S1). We then used these samples first to see whether the corpus and antrum metabolite differences were stable across this time course. Generally, as the infection proceeded, there were fewer compounds that differed between the two regions. Using the full set of different compounds (not FDR corrected), the differing metabolites decreased from 37 to 14, 25, and 29 at the 3-day, 28-day, and 8-month time points, respectively (see Table S10 in the supplemental material). Compounds that were consistently distinct between the corpus and antrum included the antrum-elevated compounds 5-methoxytryptamine, lactic acid, and the fatty acid caprylic/octanoic acid. Chemicals that were regularly more abundant in the corpus included multiple products that derive from phospholipids, including arachidonic acid, linoleic acid, oleic acid, and glycerol alpha phosphate (Table S10). Lastly, several compounds were distinct at the outset, before infection, but became increasingly similar between regions after infection, including monoacylglycerol 2-monopalmitin (also called glyceryl 2-palmitate), the sugars glucose and sucrose, and the carboxylic acids pyruvic acid and succinic acid. Taken together, these data suggest that the corpus and antrum remain distinct throughout the infection with relatively modest changes but may become slightly more similar over time.

Tissue changes over the course of an infection. As described above, we collected tissue from mice infected for varying lengths of time. Initially, we hoped to compare all of these samples, but we were not able to do this because the metabolomics analyses were run on separate days and no normalization methods could remove the analysis day bias. We therefore compared age-matched uninfected samples with 8-month

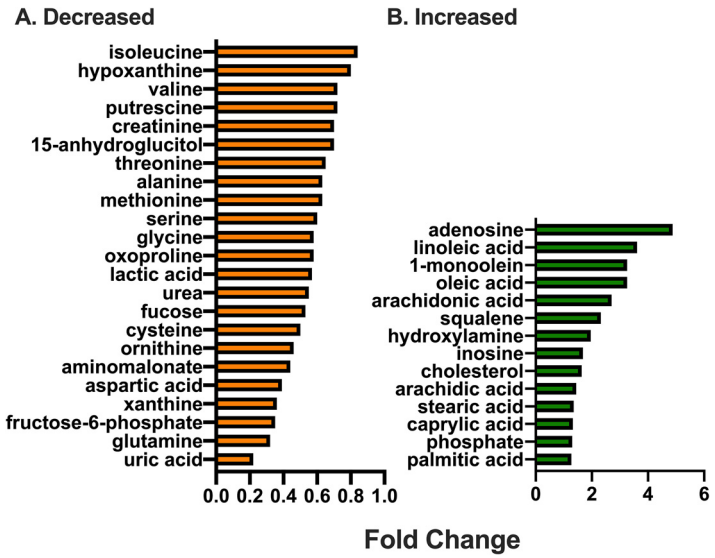

FIG 6 Corpus metabolites whose changes were highly significant between uninfected and 8-month infected mice. $n = 6$ mice per group.

infected samples and 3-day infected samples with 28-day infected samples because these sample metabolomes were analyzed together. Overall, the antral tissue remained stable, with no highly significant metabolite changes between 0 and 8 months and between 3 and 28 days (see Table S11 in the supplemental material). The only significant differences detected were in the corpus, specifically comparing uninfected tissue to 8-month infected tissue. In this case, there were 37 identified compounds that were highly significantly different (Fig. 6) and 61 compounds that were significantly different (see Table S12 in the supplemental material). Compounds that substantially increased during this time included a nearly 5-fold increase in adenosine, several lipids including those related to phospholipids (arachidonic acid, its product arachidic acid, oleic acid, linoleic acid), the lipid 1-monoolein, and the cholesterol precursor squalene. Additionally, there were ~1.5- to 2-fold increases in the ATP product inosine and the inorganic compound hydroxylamine. Compounds that decreased included the purine derivative uric acid, several amino acids (glutamine, aspartic acid, ornithine, aminomalonate), and the sugar fructose-6-phosphate. With the exception of uric acid and aspartic acid, these changes were not seen in the antrum. These data suggest that the antrum metabolome remains remarkably stable in the face of an *H. pylori* infection. The corpus, in contrast, displays several changes between the uninfected and chronically infected mice. These include indicators of possible tissue damage at the later time points as well as depletion of key nutrients, such as glutamine and fructose-6-phosphate, that support cell proliferation.

DISCUSSION

We report the metabolomic differences that exist between gastric corpus and antral organoid-secreted products and gastric tissues and how these two metabolomes respond to *H. pylori* infection. The gastric organoid data are the most straightforward to interpret because we were able to analyze extracellular molecules. We find that *H. pylori* infection leads to lower abundance of specific metabolites in both the corpus and antrum, and these lost metabolites do not differ much between these regions. One challenge with these experiments is that we can only detect presence/absence and so are unable to differentiate between increased metabolite utilization by either *H. pylori* or the mammalian cells, altered metabolite production, or altered metabolite secretion. This caveat is an important one. Our results are consistent, however, with the idea that the preferred carbon and energy sources of *H. pylori* are the carboxylic acids lactic acid, lactamide, fumaric acid, malic acid, and citric acid as well as the amino acids glutamine,

serine, *N*-acetylglutamate, aspartic acid, oxoproline/pyroglutamic acid, and tyrosine. The simplest interpretation is that these compounds are used by *H. pylori*, an idea that is supported by the decrease in compounds that are known to be used by *H. pylori*, such as urea, glutamine, cholesterol, lactic acid, and fumaric acid.

Surprisingly, little is known about the preferred nutrient and energy sources of *H. pylori* when confronted with a complex mixture. Several studies support that the microbe does not substantially rely on sugars, such as glucose, and instead relies on amino acids and carboxylic acids (31–33). Previous work supports the catabolism of carboxylic acids that we also show are depleted here. *H. pylori* can catabolize fumaric acid (34), malic acid (28), and lactic acid (25). Catabolism of carboxylic acids requires first their uptake. *H. pylori* has a C_4-dicarboxylate transport protein that takes up fumaric acid and malic acid but not the larger citric acid (35). Citric acid complexes with iron, and there are several known ferric and ferrous citrate uptake systems that have been characterized for their iron uptake properties but also presumably that bring citrate into the cell (36). Lactic acid has a separate uptake system, the LctP lactate permeases. *H. pylori* actually has two lactate permease genes, *lctP1* (HP0140) and *lctP2* (HP0141), which are encoded next to each other in the genome (25). Studies have shown that these two proteins are needed for lactate uptake but have not yet determined if they play distinct roles.

Another finding from this work is that amino acids are depleted upon *H. pylori* infection. Amino acids can act as carbon, nitrogen, and energy sources. Work using defined medium determined that there are several *H. pylori* essential amino acids (e.g., arginine, histidine, leucine, methionine, phenylalanine, and valine), with others showing cross-study variation (alanine, cysteine, proline, serine, and isoleucine) (27), but for the most part, these were not the ones that were depleted here. Instead, it seems most likely that our depleted amino acids are carbon/nitrogen or energy sources. This idea agrees well with findings that *H. pylori* can catabolize amino acids as sole carbon/energy sources for growth (33). Specifically, *H. pylori* catabolizes a large number of amino acids with the most substantial being alanine, arginine, asparagine, aspartate, glutamate, glutamine, proline, and serine, with studies reporting variation in the use of alanine, glycine, and valine (28, 33, 37, 38). This list is consistent with the amino acids depleted in this work, although we did not detect depletion of all of these and additionally found depletion of tyrosine and the glutamate derivatives *N*-acetylglutamate and pyroglutamic acid/oxoproline. *H. pylori* has several transporters that can take up amino acids, including GltS for glutamate and DcuA for aspartate (39). These same transporters also take up glutamine and asparagine after they are deamidated to glutamate and aspartate. Other known transporters include those for peptides, Dpp and Opp (40, 41). There remain several unknowns. For serine, there is a predicted but as yet uncharacterized serine uptake transporter (*sdaC* [HP0133]), there is no predicted tyrosine transporter, and it is not yet known whether GltS can take up glutamate derivatives like *N*-acetylglutamate or pyroglutamic acid.

The mouse gastric tissue analysis uncovered that the antral metabolome is surprisingly stable over the course of an 8-month infection, while the corpus showed significant changes. Another study analyzed the mouse gastric metabolome over an infection time course but did not separate the corpus and the antrum (13). These authors also found relatively minimal changes in the mouse gastric metabolome over time. Our data suggest the infected corpus tissue may have hallmarks of damage, including elevated phospholipid products and adenosine, as well as depletion of important nutrients, including the amino acids glutamine, aspartic acid, and the sugar fructose-6-phosphate. *H. pylori* has been shown to use chemotaxis to preferentially colonize sites of gastric injury, further suggesting that these changes could lead to accumulation of *H. pylori* in the corpus region (42). Taken together, the metabolomics supports the idea that the corpus is undergoing atrophy, a known *H. pylori*-associated condition (43), and indeed that released phospholipids may be early indicators of carcinogenesis (44). Adenosine has immunosuppressive properties and also has been associated with cancer development (45, 46). Thus, the data might suggest that the *H.*

pylori mouse model develops signs of carcinogenesis, cell damage, and immunosuppression that can be detected using metabolomics.

In summary, our studies suggest that *H. pylori* infection results in loss of multiple carboxylic acids and amino acids in both the corpus and the antral organoids, with minimal difference in metabolite usage between the two epithelia. We also find that there is very little overlap between the metabolites detected in the gastric organoid and tissue systems, reflecting the challenges of comparing the two systems. Lastly, we report that the antral metabolome is surprisingly stable over an 8-month *H. pylori* infection period, while the corpus displays significant changes that may indicate an early carcinogenic process.

MATERIALS AND METHODS

***H. pylori* strains and growth conditions.** *H. pylori* strain SS1 with the green fluorescent protein (GFP)-expressing plasmid pTM115 was used for all studies (9, 47, 48). *H. pylori* was grown at 37°C, 5% O_2, and 10% CO_2 (balance N_2). For solid medium, we used Columbia blood agar (BD Diagnostics, Fisher Scientific) with 5% difibrinated horse blood (Hemostat Labs, Dixon, California), 50 μg/ml cycloheximide (VWR), 10 μg/ml vancomycin, 5 μg/ml cefsulodin, 2.5 units/ml polymyxin B (all from Gold Biotechnology, St. Louis, MO), and 0.2% (wt/vol) β-cyclodextrin (Spectrum Labs, Gardena, CA) (CHBA). For liquid medium, we used brucella broth (BBL) medium supplemented with 10% heat-inactivated fetal bovine serum (FBS, Life Technologies) (BB10). For metabolomics analysis, *H. pylori* was grown in BB10 and then added to the organoids or the organoid medium for 24 h. Medium was filtered to remove bacterial cells as described below.

Organoid preparation. All organoids and tissues were prepared from female C57BL/6N mice (*Helicobacter*-free; Charles River). The University of California, Santa Cruz (UCSC) Institutional Animal Care and Use Committee approved all animal protocols and experiments (protocol number OTTEK1505). All animal procedures were in strict accordance with the NIH Guide for the Care and Use of Laboratory Animals. Mice were housed at the UCSC animal facility and given free access to food and water. For gastric organoids, 12-week-old mice were sacrificed by CO_2 narcosis, and the stomach was removed by cutting at the stomach-esophageal junction and the antrum-duodenum sphincter. The forestomach was removed and the stomach opened along the lesser curvature using scissors. The stomach was gently rinsed by moving back and forth in 25 ml ice-cold phosphate-buffered saline (PBS). Blood vessels and the muscle layer were removed from the nonluminal side of the tissue using microscissors (Kelly Scientific) and tweezers. The corpus was separated from the antrum with a scalpel based on the difference in tissue coloration as a marker for the border between these regions as described previously (49), excluding an ~5-mm section between the two tissues to ensure purity. Each piece was further divided into thirds to be used for organoid preparation, bacterial enumeration, or flash frozen in liquid N_2 for metabolomics analysis.

Organoids were isolated using a protocol adapted from Mahé et al. (50). Dissected gastric tissue was cut into 1-mm^2 pieces and incubated with slight shaking in Dulbecco's phosphate buffered saline (DPBS; Millipore) with 5 mM ETDA at 4°C for 2 h. After this period, the tissue was transferred into ice-cold DPBS containing 1% sucrose and 1.5% sorbitol and shaken roughly by hand for 2 min. The remaining large tissue pieces were allowed to settle, and 2 ml of the solution containing the glands was removed. Glands were washed with cold DPBS and mixed into 50 μl of Matrigel (BD Biosciences). Matrigel and glands were placed into a 24-well plate if being prepared for flat organoids and incubated for 10 min at 37°C until the Matrigel solidified. Three-dimensional (3D) gastric organoid medium was then added to cover the Matrigel and the glands. The 3D gastric organoid medium contains advanced DMEM/F12 (Invitrogen) supplemented with 2 mM GlutaMax (Invitrogen), 10 mM HEPES (Sigma), 100 U/ml penicillin/100 μg/ml streptomycin (Invitrogen), 1× N2 supplement (Invitrogen), 1× B27 supplement (Invitrogen), 1 μg/ml mouse R-Spondin (R&D Systems), 100 ng/ml Noggin (PeproTech), 50 ng/ml epidermal growth factor (EGF; Peprotech). Medium was exchanged with fresh medium every 2 days for up to 7 days. Under these conditions, both types of organoids grew at the same rate.

To create 2D organoids, equal volumes of spheroid gastric organoids were collected with ice-cold DPBS, the Matrigel removed by washing, and centrifugation at 195 × *g* for 5 min at 4°C. Organoids were collected and resuspended in 500 μl 2D culture medium (DMEM/F12, advanced base medium, 10% fetal bovine serum, 10 mM HEPES, 2 mM glutamine, 1× N2 supplement, 1× B27 supplement, 10 μM Y compound [Y-27632; Sigma], 50 ng/ml EGF) and placed into a collagen-coated 24-well plate for attachment. After 24 h, the medium was replaced with fresh 2D culture medium plus 1×10^7 *H. pylori* SS1 pTM115 per well. The *H. pylori* was grown in BB10 as above. After 24 h of infection, medium was collected from the organoids or bacterial cells, passed through a 0.2-μm filter to remove organoid and bacterial cells from the medium, and quick-frozen in liquid N_2. For this analysis, we had 6 independent samples for most groups (corpus infected, corpus uninfected, antrum infected, antrum uninfected, and the *H. pylori* alone control) and 3 independent samples for the medium alone.

Mouse tissue collection and preparation. Female C57BL/6N mice (Charles River) were infected at 4 to 6 weeks of age with 500 μl *H. pylori* SS1 pTM115 grown in BB10 medium to mid-exponential phase (optical density at 600 nm [OD_{600}], ~0.3). Infection was accomplished by oral infection with a 20-gauge by 1.5-in. feeding needle (Popper). At the desired time, the mouse stomachs were collected as for organoids and divided into corpus and antrum. For metabolomics, pieces were flash frozen in liquid N_2. For bacterial number determination, the piece was weighed, homogenized using the Bullet Blender (Next

Advance) with 1.0-mm zirconium silicate beads, diluted, and plated on CHBA with the addition of 20 μg/ml bacitracin, 10 μg/ml nalidixic acid, and 15 μg/ml kanamycin.

Metabolomic profiling. Samples for metabolomics were quick-frozen in liquid N_2, stored at −80°C, and shipped on dry ice to the UC Davis NIH West Coast Metabolomics Center (https://metabolomics.ucdavis.edu). Five milligrams of tissue sample or 20 μl of medium sample were mixed with 1 ml of 3:3:2 solvent (acetonitrile/isopropyl alcohol/H_2O, vol/vol/vol) and three 3-mm grinder balls. Samples were mixed for 30 s at 1,500 rpm in a Spex SamplePrep Geno/Grinder. After that, the samples were vortexed at room temperature and then shaken at 4°C for 6 min using Torrey Pines Scientific Digital Orbital Mixing Dry Baths. Finally, the samples were centrifuged at 14,000 relative centrifugal force (RCF) for 2 min, and half of the supernatant was loaded onto a gas chromatography (GC) column for untargeted analysis of primary metabolites using automatic liner exchange chromatography and cold injection GC-time of flight (TOF) mass spectrometry methods as detailed in Fiehn et al. (51). Briefly, the GC column was a GC Restek Corporation Rtx-5Sil MS column with a mobile phase of helium with automatic liner exchanges after each set of 10 injections. Mass spectrometry parameters were as follows: a Leco Pegasus IV mass spectrometer is used with unit mass resolution at 17 spectra s^{-1} from 80 to 500 Da at −70 eV ionization energy and 1,800 V detector voltage with a 230°C transfer line and a 250°C ion source. ChromaTOF version 2.32 was used for data preprocessing without smoothing, 3-s peak width, baseline subtraction just above the noise level, and automatic mass spectral deconvolution and peak detection at signal/noise levels of 5:1 throughout the chromatogram. Apex masses are reported for use in the BinBase algorithm. Result *.txt files are exported to a data server with absolute spectra intensities and further processed by a filtering algorithm implemented in the metabolomics BinBase database. The BinBase algorithm (rtx5) used the following settings: validity of chromatogram (<10 peaks with intensity >10^7 counts s^{-1}), unbiased retention index marker detection (MS similarity > 800, validity of intensity range for high *m/z* marker ions), and retention index calculation by 5th order polynomial regression. Spectra are cut to 5% base peak abundance and matched to database entries from most to least abundant spectra using the following matching filters: retention index window, ±2,000 units (equivalent to about ±2-s retention time); validation of unique ions and apex masses (unique ion must be included in apexing masses and present at >3% of base peak abundance); and mass spectrum similarity must fit criteria dependent on peak purity and signal/noise ratios and a final isomer filter. Failed spectra are automatically entered as new database entries if signal to noise is >25, purity is <1s.0, and presence in the biological study design class was >80%. All thresholds reflect settings for ChromaTOF version 2.32. Quantitative data are reported as relative peak intensities (for example, normalized to the peak intensities found in quality control samples). Data are given with the following information: (i) the BinBase name, which includes a name if the peak has been identified, or just a BinBase number/BBID if it is not identified; (ii) retention index (ret index); (iii) "quant mz'" column, which details the *m/z* value that was used to quantify the peak height of each entry; (iv) "mass spec" column, which details the complete mass spectrum of the metabolite given as mz (intensity values separated by spaces); (v) for identified compounds, external database identifiers such as InChI key defined by the IUPAC and NIST consortia, PubChem ID (the unique identifier of a metabolite in the PubChem database), and KEGG ID (gives the unique identifier associated with an identified metabolite in the community database KEGG LIGAND DB). The "internal standard" addition within the BinBase name clarifies if a specific chemical has been added into the extraction solvent as an internal standard. These internal standards serve as retention time alignment markers for quality control purposes and for quantification corrections. The full organoid metabolomics data are given in Data Set S1 in the supplemental material, and the full mouse tissue metabolomics is given as Data Set S2 in the supplemental material.

Metabolomics statistical analysis. For normalization, a variant of a "vector normalization" was calculated, in which the sum of all peak heights for all identified metabolites was calculated for each sample to create the value called mTIC (52). All mTIC averages were then compared. If these averages differ by a *P* value of <0.05, data were normalized to the average mTIC of each group; this was the case for the mouse tissue data. If averages between treatment groups are not different, data were normalized to the total average mTIC; this was the case for the organoid data. For principal-component analysis (PCA), we applied $\log_{10}$ transformation and autoscaling to the data. Difference comparisons between multiple groups were made using a one-way analysis of variance (ANOVA) or between two groups using the Student's *t* test. To control the false-discovery rate (FDR), we adjusted the *P* values using the Benjamini-Hochberg procedure (17). The mean fold change was calculated for each pair of two groups using nontransformed data. To generate the cluster analysis heat map shown in Fig. 2, the known chemical peak height from the organoid data was submitted to MetaboAnalyst (https://www.metaboanalyst.ca/) heatmap and clustering analysis. The following parameters were used: concentrations, samples in columns unpaired, data normalization by sum, and autoscaling. For output, we chose the top 40 by ANOVA.

Enrichment analysis. Chemical similarly enrichment analysis was performed using the ChemRICH approach (http://chemrich.us) (18) with the Mann-Whitney U test *P* values and median fold changes of our identified metabolites. ChemRICH was implemented using the Kolmogorov-Smirnov test on the identified clusters to evaluate whether a metabolite cluster was represented more than expected by chance.

SUPPLEMENTAL MATERIAL

Supplemental material is available online only.

SUPPLEMENTAL FILE 1, PDF file, 0.6 MB.

SUPPLEMENTAL FILE 2, XLSX file, 0.3 MB.

SUPPLEMENTAL FILE 3, XLSX file, 0.2 MB.

ACKNOWLEDGMENTS

The authors are grateful to Eitaro Aihara and Chip Montrose (University of Cincinnati) for gastric organoid culture training and advice, Andrew Liu and Kyle Kaminski (UC Santa Cruz) for experimental assistance, and Kevin Johnson and Shuai Hu (UC Santa Cruz) for comments on the manuscript.

The work described here was supported by National Institutes of Health National Institute of Allergy and Infectious Diseases grant RO1AI116946 (to K.M.O.), the National Institutes of Health National Institute of Diabetes and Digestive and Kidney Diseases grant R01DK083402 (to Y.Z.), the California Cancer Research Coordinating Committee grant CRC-15-380545 (to K.M.O.), and a postdoctoral fellowship from Leopoldina (to D.K.).

The funders had no role in study design, data collection and interpretation, or the decision to submit the work for publication.

REFERENCES

1. Choy M, Switzer P, De Martel C, Parsonnet J. 2008. Estimating disease prevalence using census data. Epidemiol Infect 136:1253–1260. https://doi.org/10.1017/S0950268807009752.
2. Brown LM. 2000. *Helicobacter pylori*: epidemiology and routes of transmission. Epidemiol Rev 22:283–297. https://doi.org/10.1093/oxfordjournals.epirev.a018040.
3. Wroblewski LE, Peek RM, Wilson KT. 2010. *Helicobacter pylori* and gastric cancer: factors that modulate disease risk. Clin Microbiol Rev 23:713–739. https://doi.org/10.1128/CMR.00011-10.
4. Yang C, Ottemann KM. 2019. Control of bacterial colonization in the glands and crypts. Curr Opin Microbiol 47:38–44. https://doi.org/10.1016/j.mib.2018.11.004.
5. Mills JC, Shivdasani RA. 2011. Gastric epithelial stem cells. Gastroenterology 140:412–424. https://doi.org/10.1053/j.gastro.2010.12.001.
6. Ding L, El-Zaatari M, Merchant JL. 2016. Recapitulating human gastric cancer pathogenesis: experimental models of gastric cancer. Adv Exp Med Biol 908:441–478. https://doi.org/10.1007/978-3-319-41388-4_22.
7. Terry K, Williams SM, Connolly LL, Ottemann KM. 2005. Chemotaxis plays multiple roles during *Helicobacter pylori* animal infection. Infect Immun 73:803–811. https://doi.org/10.1128/IAI.73.2.803-811.2005.
8. Rolig AS, Shanks J, Carter JE, Ottemann KM. 2012. *Helicobacter pylori* requires TlpD-driven chemotaxis to proliferate in the antrum. Infect Immun 80:3713–3720. https://doi.org/10.1128/IAI.00407-12.
9. Keilberg D, Zavros Y, Shepherd B, Salama NR, Ottemann KM. 2016. Spatial and temporal shifts in bacterial biogeography and gland occupation during the development of a chronic infection. mBio 7:e01705-16. https://doi.org/10.1128/mBio.01705-16.
10. Rieder G, Merchant J, Haas R. 2005. *Helicobacter pylori* cag-type IV secretion system facilitates corpus colonization to induce precancerous conditions in Mongolian gerbils. Gastroenterology 128:1229–1242. https://doi.org/10.1053/j.gastro.2005.02.064.
11. Uemura N, Okamoto S, Yamamoto S, Matsumura N, Yamaguchi S, Yamakido M, Taniyama K, Sasaki N, Schlemper RJ. 2001. *Helicobacter pylori* infection and the development of gastric cancer. N Engl J Med 345:784–789. https://doi.org/10.1056/NEJMoa001999.
12. Atherton JC. 2006. The pathogenesis of *Helicobacter pylori*-induced gastro-duodenal diseases. Annu Rev Pathol 1:63–96. https://doi.org/10.1146/annurev.pathol.1.110304.100125.
13. Nishiumi S, Yoshida M, Azuma T. 2017. Alterations in metabolic pathways in stomach of mice infected with *Helicobacter pylori*. Microb Pathog 109:78–85. https://doi.org/10.1016/j.micpath.2017.05.027.
14. Huang S, Guo Y, Li Z, Zhang Y, Zhou T, You W, Pan K, Li W. 2020. A systematic review of metabolomic profiling of gastric cancer and esophageal cancer. Cancer Biol Med 17:181–198. https://doi.org/10.20892/j.issn.2095-3941.2019.0348.
15. Chan AW, Gill RS, Schiller D, Sawyer MB. 2014. Potential role of metabolomics in diagnosis and surveillance of gastric cancer. World J Gastroenterol 20:12874–12882. https://doi.org/10.3748/wjg.v20.i36.12874.
16. Schumacher MA, Aihara E, Feng R, Engevik A, Shroyer NF, Ottemann KM, Worrell RT, Montrose MH, Shivdasani RA, Zavros Y. 2015. The use of murine-derived fundic organoids in studies of gastric physiology. J Physiol 593:1809–1827. https://doi.org/10.1113/jphysiol.2014.283028.
17. Benjamini Y, Hochberg Y. 1995. Controlling the false discovery rate: a practical and powerful approach to multiple testing. J R Stat Soc: Series B (Methodological) 57:289–300. https://doi.org/10.1111/j.2517-6161.1995.tb02031.x.
18. Barupal DK, Fiehn O. 2017. Chemical similarity enrichment analysis (ChemRICH) as alternative to biochemical pathway mapping for metabolomic datasets. Sci Rep 7:14567. https://doi.org/10.1038/s41598-017-15231-w.
19. Bertaux-Skeirik N, Feng R, Schumacher MA, Li J, Mahé MM, Engevik AC, Javier JE, Peek RM, Ottemann K, Orian-Rousseau V, Boivin GP, Helmrath MA, Zavros Y. 2015. CD44 plays a functional role in *Helicobacter pylori*-induced epithelial cell proliferation. PLoS Pathog 11:e1004663. https://doi.org/10.1371/journal.ppat.1004663.
20. Chakrabarti J, Zavros Y. 2020. Generation and use of gastric organoids for the study of *Helicobacter pylori* pathogenesis. Methods Cell Biol 159:23–46. https://doi.org/10.1016/bs.mcb.2020.04.011.
21. Huang JY, Sweeney EG, Sigal M, Zhang HC, Remington SJ, Cantrell MA, Kuo CJ, Guillemin K, Amieva MR. 2015. Chemodetection and destruction of host urea allows *Helicobacter pylori* to locate the epithelium. Cell Host Microbe 18:147–156. https://doi.org/10.1016/j.chom.2015.07.002.
22. Mizote T, Yoshiyama H, Nakazawa T. 1997. Urease-independent chemotactic responses of *Helicobacter pylori* to urea, urease inhibitors, and sodium bicarbonate. Infect Immun 65:1519–1521. https://doi.org/10.1128/IAI.65.4.1519-1521.1997.
23. Chevalier C, Thiberge JM, Ferrero RL, Labigne A. 1999. Essential role of *Helicobacter pylori* gamma-glutamyltranspeptidase for the colonization of the gastric mucosa of mice. Mol Microbiol 31:1359–1372. https://doi.org/10.1046/j.1365-2958.1999.01271.x.
24. Shibayama K, Wachino J-I, Arakawa Y, Saidijam M, Rutherford NG, Henderson PJF. 2007. Metabolism of glutamine and glutathione via gamma-glutamyltranspeptidase and glutamate transport in *Helicobacter pylori*: possible significance in the pathophysiology of the organism. Mol Microbiol 64:396–406. https://doi.org/10.1111/j.1365-2958.2007.05661.x.
25. Iwatani S, Nagashima H, Reddy R, Shiota S, Graham DY, Yamaoka Y. 2014. Identification of the genes that contribute to lactate utilization in *Helicobacter pylori*. PLoS One 9:e103506. https://doi.org/10.1371/journal.pone.0103506.
26. Takahashi T, Matsumoto T, Nakamura M, Matsui H, Tsuchimoto K, Yamada H. 2007. L-lactic acid secreted from gastric mucosal cells enhances growth of Helicobacter pylori. Helicobacter 12:532–540. https://doi.org/10.1111/j.1523-5378.2007.00524.x.
27. Testerman TL, Conn PB, Mobley HLT, McGee DJ. 2006. Nutritional requirements and antibiotic resistance patterns of *Helicobacter* species in chemically defined media. J Clin Microbiol 44:1650–1658. https://doi.org/10.1128/JCM.44.5.1650-1658.2006.
28. Lee WC, Goh KL, Loke MF, Vadivelu J. 2017. Elucidation of the metabolic network of *Helicobacter pylori* J99 and Malaysian clinical strains by phenotype microarray. Helicobacter 22:e12321. https://doi.org/10.1111/hel.12321.
29. Testerman TL, McGee DJ, Mobley HL. 2001. Helicobacter pylori growth and urease detection in the chemically defined medium Ham's F-12

nutrient mixture. J Clin Microbiol 39:3842–3850. https://doi.org/10.1128/JCM.39.11.3842-3850.2001.
30. Hirai Y, Haque M, Yoshida T, Yokota K, Yasuda T, Oguma K. 1995. Unique cholesteryl glucosides in *Helicobacter pylori*: composition and structural analysis. J Bacteriol 177:5327–5333. https://doi.org/10.1128/jb.177.18.5327-5333.1995.
31. Kelly DJ. 1998. The physiology and metabolism of the human gastric pathogen *Helicobacter pylori*. Adv Microb Physiol 40:137–189. https://doi.org/10.1016/s0065-2911(08)60131-9.
32. Marais A, Mendz GL, Hazell SL, Mégraud F. 1999. Metabolism and genetics of *Helicobacter pylori:* the genome era. Microbiol Mol Biol Rev 63:642–674. https://doi.org/10.1128/MMBR.63.3.642-674.1999.
33. Mendz GL, Hazell SL. 1995. Aminoacid utilization by *Helicobacter pylori*. Int J Biochem Cell Biol 27:1085–1093. https://doi.org/10.1016/1357-2725(95)00069-2.
34. Mendz GL, Hazell SL. 1993. Fumarate catabolism in *Helicobacter pylori*. Biochem Mol Biol Int 31:325–332.
35. Mendz GL, Meek DJ, Hazell SL. 1998. Characterization of fumarate transport in *Helicobacter pylori*. J Membr Biol 165:65–76. https://doi.org/10.1007/s002329900421.
36. Velayudhan J, Hughes NJ, McColm AA, Bagshaw J, Clayton CL, Andrews SC, Kelly DJ. 2000. Iron acquisition and virulence in *Helicobacter pylori*: a major role for FeoB, a high-affinity ferrous iron transporter. Mol Microbiol 37:274–286. https://doi.org/10.1046/j.1365-2958.2000.01987.x.
37. Stark RM, Suleiman MS, Hassan IJ, Greenman J, Millar MR. 1997. Amino acid utilisation and deamination of glutamine and asparagine by *Helicobacter pylori*. J Med Microbiol 46:793–800. https://doi.org/10.1099/00222615-46-9-793.
38. Nagata K, Nagata Y, Sato T, Fujino MA, Nakajima K, Tamura T. 2003. L-Serine, D- and L-proline and alanine as respiratory substrates of *Helicobacter pylori*: correlation between in vitro and in vivo amino acid levels. Microbiology (Reading) 149:2023–2030. https://doi.org/10.1099/mic.0.26203-0.
39. Leduc D, Gallaud J, Stingl K, de Reuse H. 2010. Coupled amino acid deamidase-transport systems essential for *Helicobacter pylori* colonization. Infect Immun 78:2782–2792. https://doi.org/10.1128/IAI.00149-10.
40. Rahman MM, Machuca MA, Khan MF, Barlow CK, Schittenhelm RB, Roujeinikova A. 2019. Molecular basis of unexpected specificity of ABC transporter-associated substrate-binding protein DppA from *Helicobacter pylori*. J Bacteriol 201:e00400-19. https://doi.org/10.1128/JB.00400-19.
41. Weinberg MV, Maier RJ. 2007. Peptide transport in *Helicobacter pylori:* roles of Dpp and Opp systems and evidence for additional peptide transporters. J Bacteriol 189:3392–3402. https://doi.org/10.1128/JB.01636-06.
42. Aihara E, Closson C, Matthis AL, Schumacher MA, Engevik AC, Zavros Y, Ottemann KM, Montrose MH. 2014. Motility and chemotaxis mediate the preferential colonization of gastric injury sites by *Helicobacter pylori*. PLoS Pathog 10:e1004275. https://doi.org/10.1371/journal.ppat.1004275.
43. Nookaew I, Thorell K, Worah K, Wang S, Hibberd ML, Sjövall H, Pettersson S, Nielsen J, Lundin SB. 2013. Transcriptome signatures in *Helicobacter pylori*-infected mucosa identifies acidic mammalian chitinase loss as a corpus atrophy marker. BMC Med Genomics 6:41. https://doi.org/10.1186/1755-8794-6-41.
44. Johnson CH, Santidrian AF, LeBoeuf SE, Kurczy ME, Rattray NJW, Rattray Z, Warth B, Ritland M, Hoang LT, Loriot C, Higa J, Hansen JE, Felding BH, Siuzdak G. 2017. Metabolomics guided pathway analysis reveals link between cancer metastasis, cholesterol sulfate, and phospholipids. Cancer Metab 5:9. https://doi.org/10.1186/s40170-017-0171-2.
45. Harvey JB, Phan LH, Villarreal OE, Bowser JL. 2020. CD73's potential as an immunotherapy target in gastrointestinal cancers. Front Immunol 11:508. https://doi.org/10.3389/fimmu.2020.00508.
46. Colgan SP, Fennimore B, Ehrentraut SF. 2013. Adenosine and gastrointestinal inflammation. J Mol Med (Berl) 91:157–164. https://doi.org/10.1007/s00109-012-0990-0.
47. Lee A, O'Rourke J, De Ungria MC, Robertson B, Daskalopoulos G, Dixon MF. 1997. A standardized mouse model of *Helicobacter pylori* infection: introducing the Sydney strain. Gastroenterology 112:1386–1397. https://doi.org/10.1016/S0016-5085(97)70155-0.
48. Amieva MR, Vogelmann R, Covacci A, Tompkins LS, Nelson WJ, Falkow S. 2003. Disruption of the epithelial apical-junctional complex by *Helicobacter pylori* CagA. Science 300:1430–1434. https://doi.org/10.1126/science.1081919.
49. Lee ER, Trasler J, Dwivedi S, Leblond CP. 1982. Division of the mouse gastric mucosa into zymogenic and mucous regions on the basis of gland features. Am J Anat 164:187–207. https://doi.org/10.1002/aja.1001640302.
50. Mahé MM, Aihara E, Schumacher MA, Zavros Y, Montrose MH, Helmrath MA, Sato T, Shroyer NF. 2013. Establishment of gastrointestinal epithelial organoids. Curr Protoc Mouse Biol 3:217–240. https://doi.org/10.1002/9780470942390.mo130179.
51. Fiehn O, Wohlgemuth G, Scholz M, Kind T, Lee DY, Lu Y, Moon S, Nikolau B. 2008. Quality control for plant metabolomics: reporting MSI-compliant studies. Plant J 53:691–704. https://doi.org/10.1111/j.1365-313X.2007.03387.x.
52. Fiehn O. 2016. Metabolomics by gas chromatography-mass spectrometry: combined targeted and untargeted profiling. Curr Protoc Mol Biol 114:30.4.1–30.4.32. https://doi.org/10.1002/0471142727.mb3004s114.
53. Xia J, Sinelnikov IV, Han B, Wishart DS. 2015. MetaboAnalyst 3.0–making metabolomics more meaningful. Nucleic Acids Res 43:W251–W257. https://doi.org/10.1093/nar/gkv380.